

Emergent Field-Driven Robot Swarm States

Gao Wang^{1,*}, Trung V. Phan^{2,*}, Shengkai Li³, Michael Wombacher¹, Junle Qu⁴, Yan Peng,⁵Guo Chen¹, Daniel I. Goldman,³ Simon A. Levin,⁶ Robert H. Austin,^{2,†} and Liyu Liu^{1,‡}¹Chongqing Key Laboratory of Soft Condensed Matter Physics and Smart Materials, College of Physics, Chongqing University, Chongqing, 400044 China²Department of Physics, Princeton University, Princeton, New Jersey 08544, USA³School of Physics, Georgia Institute of Technology, Atlanta, Georgia 30332, USA⁴Key Laboratory of Optoelectronics Devices and Systems of Ministry of Education/Guangdong Province, College of Physics and Optoelectronic Engineering, Shenzhen University, Shenzhen, 518060 China⁵Research Institute of USV Engineering, Shanghai University, Shanghai, 200444 China⁶Department of Environmental and Evolutionary Biology, Princeton University, Princeton New Jersey 08544, USA

(Received 24 September 2020; revised 22 December 2020; accepted 15 February 2021; published 12 March 2021)

We present an ecology-inspired form of active matter consisting of a robot swarm. Each robot moves over a planar dynamic resource environment represented by a large light-emitting diode array in search of maximum light intensity; the robots deplete (dim) locally by their presence the local light intensity and seek maximum light intensity. Their movement is directed along the steepest local light intensity gradient; we call this emergent symmetry breaking motion “field drive.” We show there emerge dynamic and spatial transitions similar to gas, crystalline, liquid, glass, and jammed states as a function of robot density, resource consumption rates, and resource recovery rates. Paradoxically the nongas states emerge from smooth, flat resource landscapes, not rough ones, and each state can directly move to a glassy state if the resource recovery rate is slow enough, at any robot density.

DOI: 10.1103/PhysRevLett.126.108002

The field of active matter [1–5] seeks to attain a fundamental understanding of collective properties that emerge in an ensemble of driven agents [6–9]. We explore here a unique form of active matter based on a combination of biological ecology [10] and robophysics [11,12]. As autonomous robots become increasingly more adaptive, it is interesting to ask if adaptive robot swarms can achieve complex or dynamic behavior [13,14]. We present here a robot swarm that emulates natural collective ensembles in that they change their environment by their very presence, and observe collective state changes as a consequence of their ability to self-modify their environment and respond to that self-modification.

Two of the innovations that distinguish our biological ecology based robot swarms from more conventional active matter systems [15] are the dynamic resource landscape and how the robots self-modify the landscape. They move over a $4.0 \times 4.0 \text{ m}^2$ light-emitting diode (LED) light board. Each robot has four downward facing single pixel RGB sensors in the base, which determine local light intensities and the gradient of the resource (Fig. 1). The sensors are at opposing quadrants on the base of the robot and detect corresponding intensities from a 2.5 mm LED pitch. Positions of the robots are observed by an overhead infrared CCD camera with resolution of 800×800 pixels. Each pixel of the camera sees a single 2.5 mm LED element of the light board; thus, positions in this Letter are given

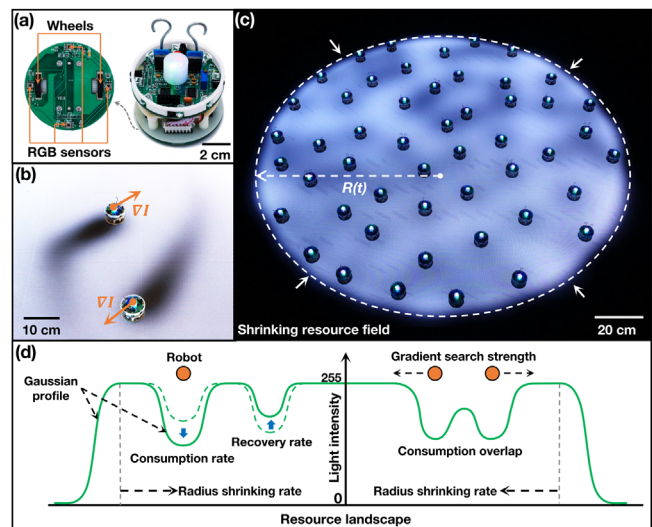


FIG. 1. Robots and the interactive LED light board environment. (a) Each robot has one microcontroller. A robot base, of diameter of 65 mm, has four RGB sensors for detection of light color from the LED light board. The movement of each robot is controlled by two independent pulse-width modulated gear motors. (b) The four RGB sensors are used to codetect gradient vectors from the underneath resource landscape. (c) The LED light board of dimension $4.0 \times 4.0 \text{ m}^2$ and 2.5 mm pitch supplies complex and dynamic environment for the robot communities. (d) The rules and parameters that control landscape resource and agents consumption property.

conveniently in terms of pixel coordinates and speeds are given in pixels/s.

Further, unlike conventional robots in a swarm, our robots have no intrinsic motion. They move only in response to a local self-generated light intensity gradient $\nabla I(x, y)$ at their positions on the light board. Gradients in the intensity emerge from depletion (dimming) of the local intensity of the resource landscape by the robots. Symmetry in the depletion hole of the local intensity $I(x, y)$ created by a stationary robot is spontaneously broken by digitization errors in the intensity detectors. This noise then bootstraps up an emergent field-drive motion. Each pixel of the local resource field shadow generated by the presence of a robot recovers with an exponential time constant τ_R once the robot moves away. The smaller τ_R is, the quicker the local resource shadow recovers. Figure 2 describes this field drive of the robots and the decaying resource shadows they leave behind.

A swarm of many field-driven robots creates an emergent complex resource field $I(x, y; t)$ which can be extremely time and space dependent, and can be quite difficult to simulate in order to compute actual robot

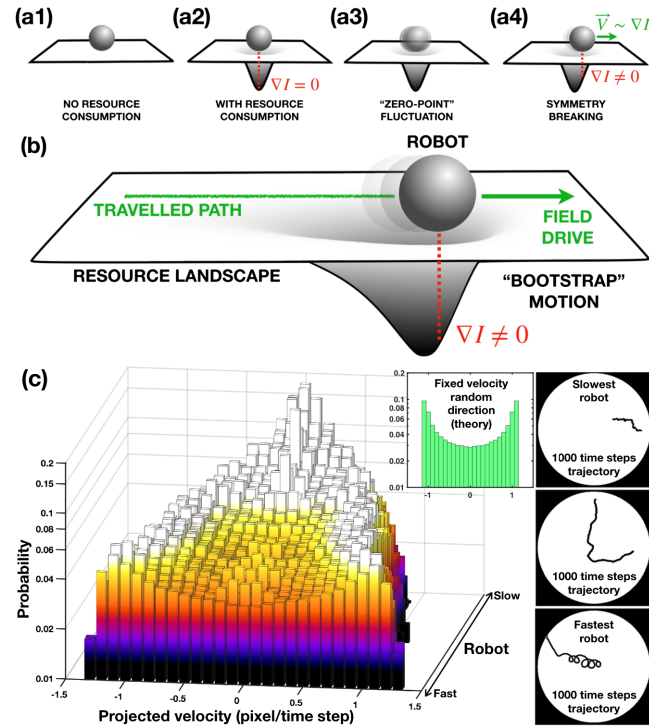


FIG. 2. Robotic field-drive emergent motion. (a1),(a2) Each robot consumes (dims) the light in a Gaussian circle around its position. (a3) Fluctuations give rise to transient intensity gradients which spontaneously give rise to a random velocity direction (a4). (b) Self-drive of a robot over an initially smooth resource field. (c) Each robot has a different response to light gradients determined by variations in the motor and drive train quality. Histogram of robot velocity distributions for all robots when moving alone in a flat landscape, ordered by their average kinetic energy, and some typical trajectories.

velocities [16]. The presence of many robots $\{j\}$ at positions $\{(x_j, y_j)\}$ on the light board gives rise to a time-dependent 2D light intensity landscape $I(x, y; t)$ across the light board:

$$\partial_t I = \frac{1}{\tau_R} (\tilde{I} - I) - \sum_j k_E e^{-[(x-x_j)^2 + (y-y_j)^2]/2\sigma^2} \Theta(I), \quad (1)$$

where τ_R is the recovery time of a pixel intensity to the robot-free intensity \tilde{I} , k_E is the characteristic resource consumption rate of a robot, σ is the radius of resource consumption, and $\Theta(\zeta)$ is a Heaviside unit step function:

$$\Theta(\zeta > 0) = 1, \quad \Theta(\zeta \leq 0) = 0. \quad (2)$$

A robot when in a position with a nonzero local resource gradient moves in response to the gradient ∇I , usually toward higher resources with velocity \vec{v}_j :

$$\vec{v}_j = \frac{dx_j}{dt} \hat{x} + \frac{dy_j}{dt} \hat{y} = \kappa \nabla I(x_j, y_j; t), \quad (3)$$

where \hat{x} , \hat{y} are unit vectors and κ is the robotic sensitivity to the landscape's local resource gradient. Computation of the magnitude of the field-drive speed of an isolated robot can be found in Supplemental Material, Sec. 1 [17]. We also show in Supplemental Material, Sec. 1.3, that in a sufficiently weak externally imposed gradient because of the local digging of resource holes that it is possible for a robot to move against a resource gradient, in the “wrong” direction. We arrive at the estimation for the maximum resource slope S a robot can move against:

$$\max |S| \approx 0.35 \frac{k_E}{U}, \quad (4)$$

where $U = \sigma/\tau_R$. This backward motion toward lower resources is critical for escape from local resource maxima which become traps due to resource hole digging.

We created heterogeneity in the robot field-drive sensitivity to mimic biological heterogeneity. The $N = 50$ robots used in these experiments have different emergent speeds because of variability in the mechanical construction, as we show in Fig. 2(c). This heterogeneity we view as an asset and not a bug: as in living systems but typically not in engineered systems, heterogeneity is the rule and not the exception.

The simplest resource landscape is a circle of light of radius R and a single resource color, namely, “white” ($I_R = I_G = I_B$). In order to study how the robot swarm behavior changed with density, we decreased the radius $R(t)$ linearly with time t :

$$R(t) = R_o(1 - \alpha t). \quad (5)$$

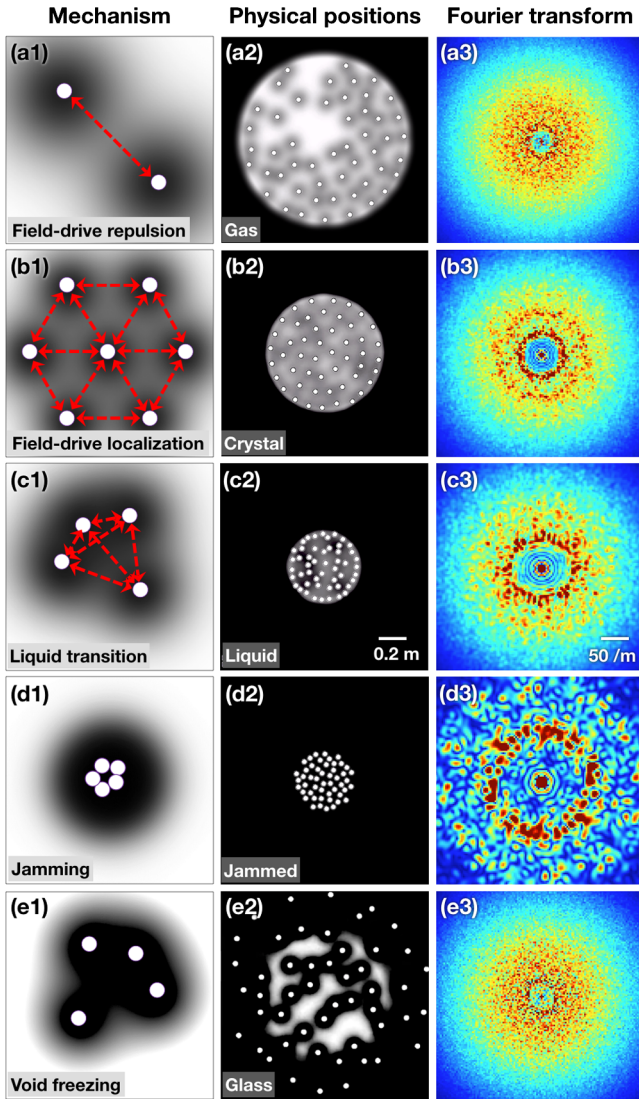


FIG. 3. The basic robot spatial distribution and the resource landscape field dynamic as the light environment radius shrinks. Column (a1)–(e1) outlines how field drive results in robot different localized states, and column (a2)–(e2) shows snapshots of robot positions in five different phases. Column (a3)–(e3) shows the spatial Fourier transformation of the robot positions in column (a2)–(e2).

In order to provide gradients at the circle perimeter, the perimeter is softened by a fixed Gaussian width $\sigma_o \ll R_o$.

The fundamental sign of the robot-robot field interaction is negative (repulsive) due to resource competition between two nearby robots, as shown in Fig. 3(a1). At relatively low robot densities the robots act like a gas of self-avoiding objects of finite size [Fig. 3(a2)]. Familiar collective patterns emerge with increasing density, such as phenomenon related to phase transitions in soft-matter physics [1]. Figures 3(b1)–3(d1) show that as the density increases, varieties of interaction modes emerge among the localized robots, thus leading to crystal, liquid, and jammed states in sequence in overall community [Figs. 3(b2)–3(d2)].

As the robot density increases, the resource landscape gets smoother since the average local consumption rate of resources increases with robot density, but the recovery rate per pixel does not. Movie 1 in Supplemental Material gives the video of 50 robots as the circle of light shrinks [17]. Figures 3(a3)–3(e3) show the density dependent structure function $S(k_x, k_y)$ [18] we get from spatial Fourier transformation of robot positions as a function of robot density.

Since we can track individual robots, it is possible to quantitatively measure the position and velocity of each robot during a compression process. We use two different order parameters to characterize the emergent phases: ψ_6 for spatial ordering and τ^* for time ordering: (1) ψ_6 .—Since circles close pack to a hexagonal array [19], a natural order parameter to characterize the initial ordering of the robots with compression is the sixfold index ψ_6 [20]:

$$\psi_6 = \left\langle \frac{1}{N_j} \sum_{j'} e^{i6\theta_{jj'}} \right\rangle_{\text{bulk}}. \quad (6)$$

The value ψ_{6j} is the local bond-orientation order parameter, where the summation j' runs over all N_j nearest neighbor of robot j . $\theta_{jj'}$ is the angle between the vector connecting robots j to j' and an arbitrary fixed reference axis. $\langle \cdot \rangle_{\text{bulk}}$ denotes averaging over all robots excluding ones near the boundary of the environment. We use Voronoi tessellation [21] to define the nearness to the boundary. (2) τ_* .—The time-correlated spatial dynamics of the robots, as distinct from their time-independent spatial correlations ψ_6 , can be captured by both the histogram of the robot kinetic energies $\langle \vec{v}_j^2 \rangle$ and the dynamic four-point susceptibility order parameter χ_4 [22,23]. χ_4 is calculated by first determining the dynamical overlap function $Q(t, \tau; a)$:

$$Q(t, \tau; a) = \frac{1}{N} \sum_{j=1}^N \Theta(a - |\vec{r}_j(t + \tau) - \vec{r}_j(t)|), \quad (7)$$

where the vector position of robot j at time t is given by

$$\vec{r}_j(t) = x_j(t)\hat{x} + y_j(t)\hat{y}, \quad (8)$$

and a is a characteristic length which is usually chosen as the radius of an agent [24]. The function $\chi_4(\tau; a)$ is then computed as the variance of $Q(t, \tau; a)$ over the quasisteady-state time interval:

$$\chi_4(\tau; a) = N \text{Var}_t(Q(t, \tau; a)). \quad (9)$$

Figure 4(c) shows the variance of $Q(t, \tau, a)$, i.e., χ_4 , for an experiment. τ_* , as shown in Fig. 4(c), can be intuitively viewed as the mean trapping *time* of a robot around a given position.

There are three parameters which control the robot swarm field-drive matter states: the areal density of the robots σ and the two field relaxation processes: the

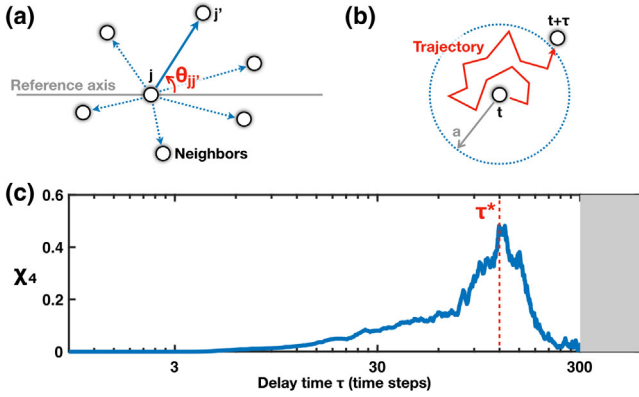


FIG. 4. (a) Demonstration for ψ_6 calculation. (b) Demonstration for χ_4 calculation. (c) An example of characteristic time τ^* evaluated from the peak position of $\chi_4(\tau, a)$.

shrinking rate of the light circle α in pixels/s and the environmental recovery time τ_R in seconds; see Movies 2 and 3 in Supplemental Material [17]. If τ_R is set too slow and/or α is set too fast, the robots simply deplete (blacken) the resources and all motion freezes out. This phenomenon that we call void freezing is a new form of a glass transition, shown in Fig. 3(e2). Remarkably, even the gas state can directly transit to the void glass state if τ_R is sufficiently slow, something that does not occur in any other forms of active matter of which we are aware.

With decreasing values of τ_R for a fixed α different phases of the field-drive matter emerge, other robot phases emerge. With increasing compression, the robots first freeze into a hexagonal crystalline state, with high ψ_6 , high τ^* , and lowered $\langle \vec{v}_j^2 \rangle$. Note that this crystalline state is at relatively low robot densities and is not a jamming transition [25] because the robots are not in contact with

each other, as is shown in the Supplemental Material, Sec. 4 [17].

The transition from a gas to a crystal state, not seen in inertially driven systems [26], emerges since our robots have no physical inertia but rather a field-driven motion. By “no physical inertia,” we mean that field drive (gradient searching of resources) gives the robots motility. In the absence of a gradient, they do not and cannot move. If we suddenly remove the gradient, the moving robots immediately stop by the next time step iteration. In that sense they have no physical inertial at all. More details can be found in Sec. 1 and Movie 4 of Supplemental Material [17].

Because of the decreasing resource landscape roughness with increasing robot density, the crystalline state pressure melts into a liquid state, with a decrease in ψ_6 , decrease in τ^* , and increase in $\langle \vec{v}_j^2 \rangle$. Melting from a crystalline to a liquid state, as explained in the Supplemental Material, Sec. 2.1 [17], requires robot escape from local resource minima due to their ability in the field-drive mechanism to move against a sufficiently weak resource gradient. Finally, the liquid state freezes in a jammed glass as the robot field drive moves the robots into contact with each other so that the state is incompressible, and the field again becomes depleted (black). The jammed state is, however, much different than the void glass freeze: the void glass state is due to the robots falling out of steady-state equilibrium. Figure. 5(a) shows the result for the spatial order parameter ψ_6 , Fig. 5(b) gives the kinetic energy v^2 distribution of robots and Fig. 5(c) presents the dynamical order parameter χ_4 mean value τ^* . Information on $\langle \vec{v}_j^2 \rangle$ with different τ_R can be found in Movie 5 and Sec. III in Supplemental Material [17].

Since this biologically inspired robot swarm active matter does not have a well-defined temperature, it is

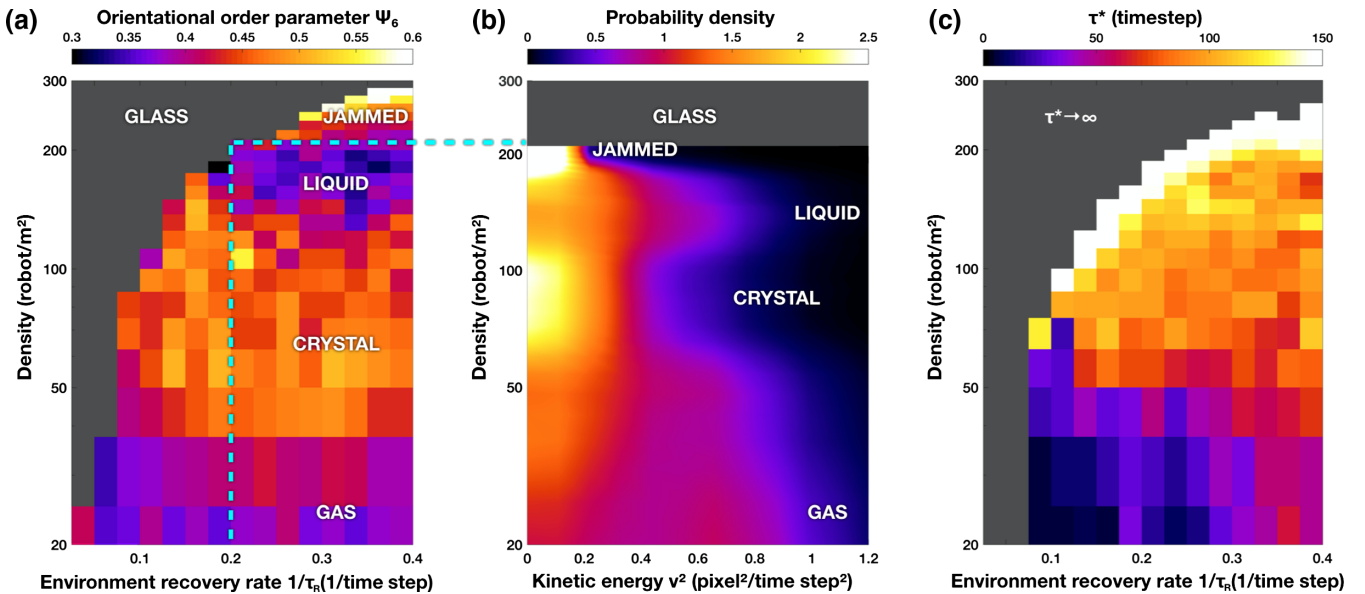


FIG. 5. (a) ψ_6 as a function of robot density and resource recovery rate $1/\tau_R$. (b) Robot kinetic energy density \vec{v}_j^2 as a function of robot density for a fixed resource recovery time of $\tau_R = 5$ time steps. (c) τ_* as a function of robot density and resource recovery rate $1/\tau_R$.

difficult to draw the usual phase diagram to show the states. A plot of the states versus the ψ_6 orientational order parameter and the susceptibility characteristic timescale τ^* [24],

$$\chi_4(\tau^*; a) = \text{Max}_\tau(\chi_4(\tau; a)), \quad (10)$$

is seen in Fig. 4(c).

Our robot field-drive and emergent states present a biologically inspired active matter. The robots remodel a resource landscape and that remodeled landscape guides the robots' locomotion, even against resource gradients. The field drive also generates a field-analog multibody interaction between the robots, as we discuss in Sec. 2 of Supplemental Material [17]; see also Refs. [27,28]. We view robots as tools for a third way of modeling dynamical systems, complementing theoretical ideas, digital computation, and now robophysical approaches. Thus robots (and robophysics [11]) provide another way to develop models of phenomena which can lead to insights in biological systems (locomotion, resource landscape utilization) as well as systems to explore interesting dynamics in physics (e.g., dynamical systems, active matter), and engineers in principle can take the robophysics insights and turn them into more interesting robots. Hopefully with better control and understanding of the collective robot responses, we will uncover potentially rich, robust, and surprising phenomena with possible connections to biology, ecology, and even sociology [29,30].

This work was supported by the NSFC (Grants No. 11974066 and No. 11674043), Capital's Funds for Health Improvement and Research (Grant No. 2020-2-2072), the U.S. National Science Foundation PHY-1659940, and the Princeton Catalysis Initiative. D. I. G was supported by U.S. Army Research Office under MURI Award No. W911NF-19-1-0233 and S. A. L. by U.S. Army Research Office Grant No. W911NF-18-1-0325. We thank Robert Axelrod, Ken Pienta, Joshua Weitz, and Tuan K. Do for helpful comments.

*These authors contributed equally to this work.

†austin@princeton.edu

‡lyliu@cqu.edu.cn

- [1] S. R. Nagel, *Rev. Mod. Phys.* **89**, 025002 (2017).
- [2] R. Zakine, J.-B. Fournier, and F. van Wijland, *Phys. Rev. Lett.* **121**, 028001 (2018).
- [3] L. Barberis and F. Peruani, *Phys. Rev. Lett.* **117**, 248001 (2016).
- [4] B. Liebchen and D. Levis, *Phys. Rev. Lett.* **119**, 058002 (2017).
- [5] M. C. Marchetti, J. F. Joanny, S. Ramaswamy, T. B. Liverpool, J. Prost, M. Rao, and R. A. Simha, *Rev. Mod. Phys.* **85**, 1143 (2013).
- [6] M. E. Cates, *Rep. Prog. Phys.* **75**, 042601 (2012).
- [7] W. C. K. Poon, *Proceedings of the International School of Physics "Enrico Fermi", Course CLXXXIV "Physics of Complex Colloid"*, edited by C. Bechinger, F. Sciortino, and P. Zihlerl (IOS, Amsterdam, 2013), pp. 317–386 [arXiv:1306.4799].
- [8] I. D. Couzin, J. Krause, N. R. Franks, and S. A. Levin, *Nature (London)* **433**, 513 (2005).
- [9] T. Vicsek and A. Zafeiris, *Phys. Rep.* **517**, 71 (2012).
- [10] M. Cenzler and L. K. M'Gonigle, *Evolution* **73**, 648 (2019).
- [11] J. Aguilar, T. N. Zhang, F. F. Qian, M. Kingsbury, B. McInroe, N. Mazouchova, C. Li, R. Maladen, C. H. Gong, M. Travers, R. L. Hatton, H. Choset, P. B. Umbanhowar, and D. I. Goldman, *Rep. Prog. Phys.* **79**, 110001 (2016).
- [12] S. Li, Y. O. Aydin, G. Small, C. Xiao, J. M. Rieser, H. N. Gynai, P. Laguna, and D. I. Goldman, arXiv:2004.03549.
- [13] M. Rubenstein, A. Cornejo, and R. Nagpal, *Science* **345**, 795 (2014).
- [14] A. Deblais, T. Barois, T. Guerin, P. H. Delville, R. Vaudaine, J. S. Lintuvuori, J. F. Boudet, J. C. Baret, and H. Kellay, *Phys. Rev. Lett.* **120**, 188002 (2018).
- [15] J. Seo, J. Paik, and M. Yim, *Annu. Rev. Control Robot. Auton. Syst.* **2**, 63 (2019).
- [16] R. Butler and M. Pennotti, 2013 Conf. Syst. Eng. Research **16**, 747 (2013).
- [17] See Supplemental Material at <http://link.aps.org/supplemental/10.1103/PhysRevLett.126.108002> for the field-drive physics, emergent states of the robot swarm, kinetic energy distribution and contact number during jamming.
- [18] P. M. Chaikin, T. C. Lubensky, and T. A. Witten, *Principles of Condensed Matter Physics* (Cambridge University Press, Cambridge, England, 1995), Vol. 10.
- [19] S. Atkinson, F. H. Stillinger, and S. Torquato, *Proc. Natl. Acad. Sci. U.S.A.* **111**, 18436 (2014).
- [20] D. Nelson, *Bond-Orientational Order in Condensed Matter Systems* (Springer Science & Business Media, New York, 2012).
- [21] D. Debnath, J. S. Gainer, C. Kilic, D. Kim, K. T. Matchev, and Y. P. Yang, *Eur. Phys. J. C* **76** (2016).
- [22] T. Reisz, *Nucl. Phys.* **B450**, 569 (1995).
- [23] J. J. Godina, Y. Meurice, M. B. Oktay, and S. Niermann, *Phys. Rev. D* **57**, 6326 (1998).
- [24] A. S. Keys, A. R. Abate, S. C. Glotzer, and D. J. Durian, *Nat. Phys.* **3**, 260 (2007).
- [25] G. Briand and O. Dauchot, *Phys. Rev. Lett.* **117** (2016).
- [26] A. Deblais, T. Barois, T. Guerin, P. H. Delville, R. Vaudaine, J. S. Lintuvuori, J. F. Boudet, J. C. Baret, and H. Kellay, *Phys. Rev. Lett.* **120**, 188002 (2018).
- [27] G. S. Fulcher, *J. Am. Ceram. Soc.* **8**, 339 (1925).
- [28] M. P. Brenner, L. S. Levitov, and E. O. Budrene, *Biophys. J.* **74**, 1677 (1998).
- [29] R. Axelrod and D. S. Bennett, *Br. J. Political Sci.* **23**, 211 (1993), <https://www.jstor.org/stable/194248>.
- [30] T. Balch, F. Dellaert, A. Feldman, A. Guillory, C. L. Isbell, Z. Khan, S. C. Pratt, A. N. Stein, and H. Wilde, *Proc. IEEE* **94**, 1445 (2006).